



DIGITAL
LIBRARY

dspace.vutbr.cz

Near-field digital holography: a tool for plasmon phase imaging

DVOŘÁK, P.; KVAPIL, M.; BOUCHAL, P.; ÉDES, Z.; ŠAMOŘIL, T.;
HRTOŇ, M.; LIGMAJER, F.; KŘÁPEK, V.; ŠIKOLA, T.

Nanoscale

2018, vol. 10, iss. 45, pp. 21363-21368

ISSN: 2040-3372

DOI: <https://doi.org/10.1039/c8nr07438k>

Accepted manuscript

Cite this: DOI: 10.1039/xxxxxxxxxx

Near-field digital holography: a tool for plasmon phase imaging[†]

Petr Dvořák,^{*a,b} Michal Kvapil,^{a,b} Petr Bouchal,^{a,b} Zoltan Édes,^{a,b} Tomáš Šamořil,^{a,b} Martin Hrtoň,^{a,b} Filip Ligmajer,^{a,b} Vlastimil Krápek,^{a,b} and Tomáš Šikola^{a,b}

Received Date

Accepted Date

DOI: 10.1039/xxxxxxxxxx

www.rsc.org/journalname

The knowledge of the phase distribution of near electromagnetic field has become very important for many applications. However, its experimental observation is still technologically very demanding task. In this work, we propose a novel method for the measurement of the phase distribution of near electric field based on the principles of phase-shifting digital holography. In contrast with previous methods the holographic interference occurs already in the near field and the phase distribution can be determined purely from the scanning near-field optical microscopy measurements without need of additional far-field interferometric methods. This opens a way towards on-chip phase imaging. We demonstrate the capabilities of the proposed method by reconstruction of the phase difference between interfering surface plasmon waves and by imaging the phase of single surface plasmon wave. We also demonstrate a selectivity of the method towards individual components of the field.

1 Introduction

An effort to measure and control the phase distribution of surface plasmon polaritons (SPPs) opened the fields of plasmon holography^{1–3}, 2D interference^{4–8}, dynamic trapping⁹ and transformation optics^{10,11}, and has become important for investigation of metamaterials^{12,13}. Though accessing the information about the phase of SPPs is much desired, its experimental determination is rather difficult. It was first measured using off-axis confocal holographic microscopy^{14,15}; nevertheless, the spatial resolution of the phase images was limited by the diffraction. Obtaining the phase of SPP below the diffraction limit was demonstrated using heterodyne scanning near-field optical microscopy (SNOM) in collecting-SNOM^{16–21} (c-SNOM) or scattering-SNOM^{22,23} (s-SNOM) configurations, using synthetic optical holography²⁴ and also via photon scanning tunneling microscopy^{25,26} (PSTM).²⁷ All these techniques collect the SPP signal in the near-field. However, the holographic interference occurs in the far field. The experimental setups thus require sophisticated interferometric configurations, where the near-field microscope is incorporated in the signal arm of the far-field interferometer.

In this paper, we present novel experimental method of near-field phase-shifting digital holography (NPDH) and demonstrate its potential for purely near-field measurements of the SPP phase distribution. The core of the proposed method is an on chip interferometer²⁸ with a signal near field and a reference near field excited by single field (in our case plane wave) to ensure their coherence. The phase of the reference field is controlled by spatial light modulator (SLM) implemented in the illumination path of the c-SNOM, allowing phase-controlled excitation of near field. We have used two specific implementation of the on-chip interferometer: a circular slit forming a standing SPP wave and a V-shaped slit forming a propagating SPP wave.

By adopting the principles of the established far-field method of phase-shifting holography^{29,30}, we generate four phase-shifted SPP interference patterns, allowing the numerical reconstruction of the phase difference of interfering SPP waves. These four interference patterns differ in the mutual phase shift between the SPPs (set by the SLM). Since all information is collected in the near-field, our method provides purely near-field measurement and avoids the use of a far-field interferometer. We stress the versatility of this method that can be directly implemented in variety of techniques capable of near-field imaging (such as SNOM, photoemission electron microscopy^{31,32} and PSTM), provided the SLM can be introduced in the illumination path. We demonstrate the utility of our method by successful reconstruction of the phase difference between the interfering SPPs. Furthermore, we show that using NPDH we are able to image not only the phase difference of interfering plasmons, but also the phase of a single SPP

* E-mail: petr.dvorak@ceitec.vutbr.cz

^a Central European Institute of Technology, Brno University of Technology, Purkyňova 123, Brno 612 00, Czech Republic.

^b Institute of Physical Engineering, Brno University of Technology, Technická 2, Brno 616 69, Czech Republic.

[†] Electronic Supplementary Information (ESI) available: [Plasmon interference for a circular slit; the tilt of sample; the experimental noise; testing the phase-controlled excitation of SPPs by the SLM]. See DOI: 10.1039/b000000x/

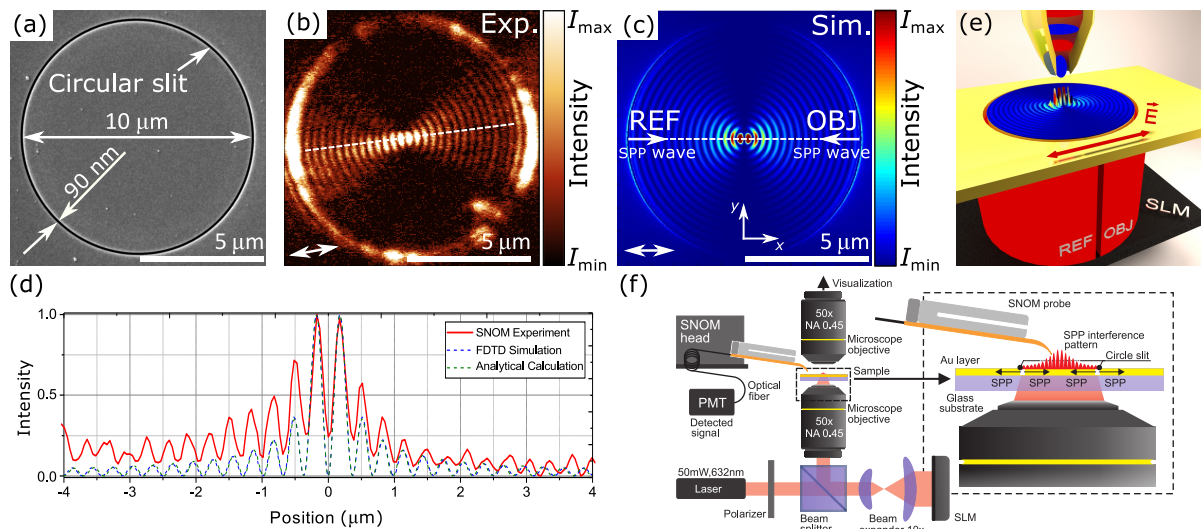


Fig. 1 (a) Scanning electron microscope image of the fabricated 90nm wide circular slit with a diameter of 10 μm . (b) SNOM image and (c) FDTD simulation of the SPP interference pattern (out-of-plane component) resulting from the laser illumination linearly polarized in the direction marked by the double arrow. (d) The intensity profiles along the dashed white line parallel with the direction of polarization. (e) Concept of near-field digital holography for plasmon phase imaging. (f) Scheme of the experimental setup.

wave without the use of heterodyne interferometry.

2 Results and discussion

As it was mentioned above, the NPDH method for obtaining the phase distribution of plasmons is based on the utilization of the interference of SPPs. For the generation of plasmons we utilize the well-known effect of plasmon excitation on illuminated slits in metallic layers.³³ Specifically, in our experiments we use polarization independent circular slits as the on-chip interferometers (diameter of 10 μm and width of 90 nm).^{34,35} The slits were milled using focused ion beam (FIB) into a 200-nm-thick gold layer on a fused silica substrate (see Fig. 1a). The SPPs are excited by linearly-polarized laser light (wavelength of 633 nm, output power of 50 mW) illuminating the slits from the bottom while the film thickness hinders the transmission of the excitation light through the gold layer.⁵ The top of the slits presents a source of SPPs propagating along the upper gold interface. By the interference of counter-propagating SPPs a standing SPP wave is formed inside the circular slit. The measured SPP interference pattern is shown in Fig. 1b. It is in a very good agreement with the calculated interference pattern (FDTD simulations and also analytical calculations, see Fig. 1d) including the varied spatial periodicity of the standing plasmon waves, i.e., a decrease from 340 nm at the center of the interference pattern to 305 nm at its edge (for details see Supplementary Information†). These experiments were performed using SNOM probes with an aperture size of 50 nm, sensitive mainly to the out-of-plane component of the field.^{27,36–38}

In order to utilize the method of NPDH for phase reconstruction we need to actively control the phase of reference SPP wave. Therefore, our setup includes a SLM, enabling us to change the phase of the illumination light across its wavefront. By the spatial alignment of the illumination beam to the circular slit we can control the phase of the light impacting different parts of the slit and the

refore also the phase of the interfering waves of SPPs. The SPPs travelling within the on-chip interferometer are given by complex amplitudes

$$U_S = A_S \exp(i\varphi_S), \quad U_{R,j} = A_R \exp[i(\varphi_R - \theta_j)]. \quad (1)$$

Using the terminology established in optical holography: A_S , φ_S and A_R , φ_R are the amplitudes and phases of signal and reference SPPs, respectively, and $\theta_j = (j-1)\pi/2$, $j = 1, 2, 3, 4$ are additional phase shifts imposed on the reference SPPs by the SLM. The interference patterns of phase-shifted SPPs are then given by intensity

$$I_j = A_R^2 + A_S^2 + 2A_R A_S \cos(\Delta\varphi + \theta_j). \quad (2)$$

The phase difference between the interfering SPP waves $\Delta\varphi = \varphi_S - \varphi_R$ is the main quantity of our interest and it can be directly obtained by substitution of the intensity records (I_1, I_2, I_3, I_4) into the formula²⁹

$$\Delta\varphi = \tan^{-1} \left(\frac{I_4 - I_2}{I_1 - I_3} \right). \quad (3)$$

In the following we demonstrate both experimentally and numerically that the phase difference of SPPs can be reconstructed from the four modified interference patterns using this simple formula.

Before the utilization of the phase-shifting procedure, we tested the phase-controlled excitation of SPPs by the SLM. The proposed masks were tested in numerical simulations based on the exact solution of the Rayleigh-Sommerfeld³⁹ diffraction integral and subsequently applied at the SLM.

In order to implement the on-chip interferometer with two counter-propagating phase-controlled SPPs, the active area of the SLM was divided into two halves (see two examples of masks in Fig. 2a). Hence, the opposite arcs of the circular slit in the direction of the polarization were illuminated with light delayed by a phase of θ_j with respect to each other. The left half of the

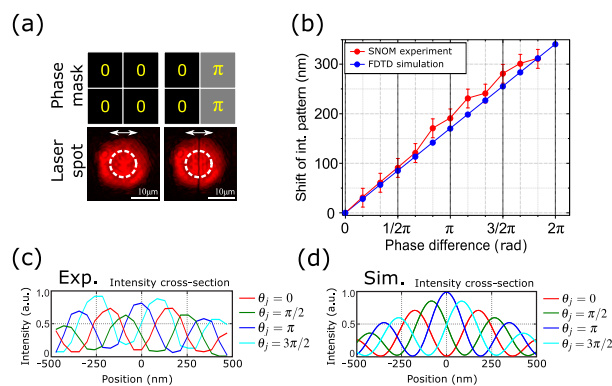


Fig. 2 (a) Two different phase mask settings and the optical image of the laser spot with the highlighted direction of the laser polarization (see the double arrow). (b) Dependence of the shift of the interference pattern on the phase difference between the SPP waves. (c) Experimental and (d) simulated intensity cross sections of the interference pattern for 4 different phase shifts.

phase mask had the zero phase-shift and in the right half we set different phase shifts between 0 and 2π with a step of $\pi/6$. A good compliance between measured and expected interference patterns demonstrates Fig. 2. The theoretical and experimental shift of the interference pattern with increasing phase delay introduced between interfering SPPs is shown in Fig. 2b, while the cross-section profiles through the central areas of experimental and simulated interference patterns for phase shifts θ_j are presented in Fig. 2c,d. It proves the functionality of the phase control of the reference wave. Furthermore, the spatial control of the phase opens up the possibility to control the pattern position with a remarkable precision making these interference structures very attractive for applications, where a precise spatial control of plasmonic fields is required.^{40,41} Our phase-shifting setup also allows to check for the tilt of the sample (for more details see the discussion in Supplementary Information†).

In the previous experiments, we have demonstrated the phase-controlled excitation of the SPPs. It allowed us to acquire phase-shifted interference patterns. To demonstrate the phase reconstruction from phase-shifted SPP interference patterns, we processed four images recorded for distinct phase shifts θ_j (Fig. 3a). The interference patterns were processed according to Eq. (3) and the phase difference $\Delta\phi$ was reconstructed. The reconstructed phase difference image is shown in Fig. 3e including the cross-section along the red dashed line. The phase difference was successfully reconstructed only in the bow-tie regions where the interference pattern has a reasonable intensity and it changes approximately from $-\pi$ to $+\pi$. The spatial periodicity of the phase difference corresponds to the periodicity of the SPP interference pattern (305 nm close to the slits and 340 nm in the center). We have followed the same phase-reconstructing procedure using FDTD simulated interference patterns, the resulting phase difference is shown in Fig. 3b. It is apparent that unlike the phase difference image from the experimental data, the reconstruction revealed the phase over the whole area inside the circular slit. Obviously it was possible due to the absence of noise in the simulated interference patterns, contrary to the measured ones. The exper-

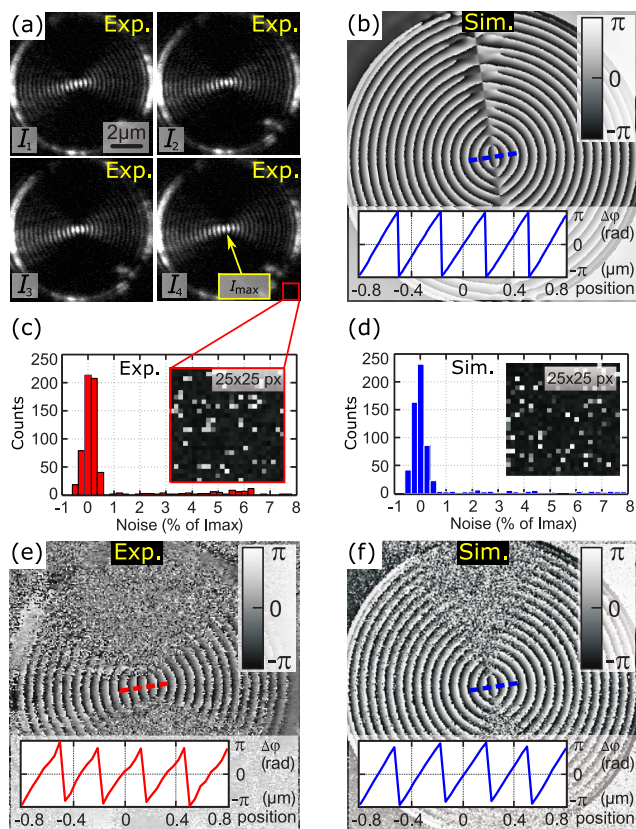


Fig. 3 SPP phase reconstruction realized by numerical processing of experimental and simulated interference patterns. (a) Measured interference patterns with the 4 distinct phase-shifts $\theta_j = 0, \pi/2, \pi, 3\pi/2$ introduced between interfering SPPs by the SLM. (b) The SPP phase difference image reconstructed by numerical processing of the FDTD simulated interference pattern. (c) Histogram showing noise which disrupts the measured data. The noise is evaluated from a (25×25) pixels area marked in (a) and expressed relative to the maximum intensity of the interference pattern. (d) Simulation of the noise distribution, (e) the SPP phase difference reconstructed by numerical processing of experimental data (interference patterns from (a)). (f) The SPP phase reconstruction with the noise model (d) applied on simulated interference patterns. The profiles in (b), (e) and (f) show cross-sections along the dashed lines in the central parts of the phase images.

imental noise was evaluated in a blank area of (25×25) pixels marked in Fig. 3a and its distribution is expressed relative to the maximum intensity of the interference pattern (Fig. 3c). We have generated a noise of the similar distribution as in experiments numerically (see Fig. 3d) and implemented into the simulated holograms. The reconstructed phase image within the bow-tie-shaped (Fig. 3f) then corresponds very well to the measured one (Fig. 3e). The influence of various levels of noise is further documented in Supplementary Information (Fig. S6†) together with the evaluation of minor distinctions between the measured and the simulated phase difference.

Using the circular interference structures we were able to demonstrate the capabilities of our NPDH method for SPP phase imaging. However, so far we have reconstructed only the phase difference between two interfering SPP waves. Next, we present a modified approach capable of direct imaging of the phase of

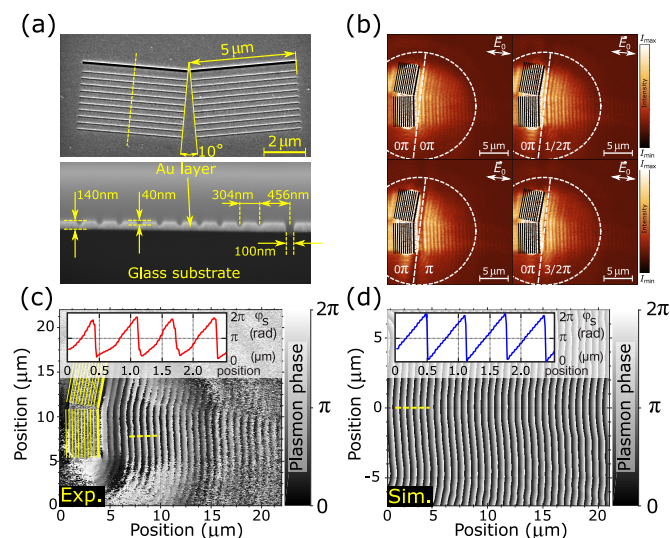


Fig. 4 (a) Top: SEM image of cosine-Gauss structures. Only the top pair of slits act as sources of SPP, the bottom slits are not fully cut through the gold layer and serve as Bragg reflectors. Bottom: Cross-section of the structures. (b) Experimental intensity distribution acquired by SNOM for four distinct phase shifts θ_j . The white dashed circle shows the laser spot with the areas of different phase of the incident light. (c), (d) Reconstructed phase image obtained from experimental (c) and calculated (d) interference patterns.

single SPP. To this end we require a reference wave with a known phase, at best constant over the entire image area. Unfortunately, SPP waves do not exhibit well defined phase due to fabrication imperfections, inhomogeneity and granularity of the metallic layer, etc. As a solution, we can utilize the illumination (laser) beam passing through the gold layer, which represents a well-defined plane wave, as a reference. From the interference of the SPP object wave with the illumination wave it is possible to reconstruct the phase of the propagating SPP wave.⁴² In order to observe this interference, the measurement setup and the sample as well needs to be slightly adjusted. First, the excitation wave has only the in-plane electric field component. Therefore, c-SNOM probes with bigger apertures have to be used, sensitive primarily to the in-plane component of the electric field.³⁸ Second, for the optimum visibility of the interference patterns the amplitude of the reference wave shall be comparable to the amplitude of the SPP. This is ensured by reducing the thickness of the gold layer to 140 nm. As the object wave, whose phase we aim to reconstruct, we used SPPs launched from a V-shaped pair of slits resulting in SPP wave similar to the so-called cosine-Gauss non-diffracting beam (see Fig. 4a).⁴³

Fig. 4b shows four experimental SNOM images with different phase shifts between the reference and object waves. The reconstructed phase image of cosine-Gauss non-diffracting beam is shown in Fig. 4c, including the line profile along the yellow dashed line. The good overall agreement between the measured and simulated results clearly shows the capability of our method to reconstruct the phase of a single SPP wave.

Finally, we address application consequences of the near-field phase-shifting digital holography. We envisage two broad application fields for the technique — near-field imaging of phase ob-

jects (biological cells and cellular structures) with excellent spatial resolution and characterization of phase-changing optical elements (plasmonic metasurfaces, superlenses, etc.).¹⁵ In combination with SNOM as a near field imaging technique, NPDH is polarization sensitive. In addition, the technique is rather versatile and not limited to SNOM. Instead, it can be combined with other near-field imaging techniques such as photoelectron emission microscopy which will then allow for ultrafast near-field phase imaging. For a generalized fully near-field operation of NPDH we propose a two-step approach. First, interferometer chip with a single slit in the gold layer is fabricated. SPP produced by the slit is characterized by NPDH using the interference with transmitted illumination wave. Second, this SPP wave is used as a reference wave (with the phase spatial distribution known from the first step) to characterize the phase of the studied object. Those objects can be for example weakly scattering biological cells or localized plasmonic modes of nanoantennas.

3 Conclusions

In summary, we have presented a new method for near-field phase imaging based on principles of phase-shifting digital holography. We have demonstrated the capabilities of our method by reconstructing the phase difference between counter-propagating SPP waves excited inside a circular slit structure. Furthermore, we have successfully reconstructed the phase of a single cosine-Gauss non-diffracting SPP wave from its interference with the exciting laser illumination. We have addressed and discussed the impact of the noise and the sample tilt which can affect the measured interference pattern and thereby the reconstructed phase images. The strength of the method lies in its compatibility with experimental techniques suitable for ultrafast SPP imaging, e.g. photoemission electron microscopy. The method presents an important step towards the development of 2D plasmonic holography for imaging of phase contrasts of objects (e.g. biological cells, plasmonic nanoantennas) bounded to surfaces.

4 Materials and methods

4.1 Experiments

Fused silica substrates were coated by a 3 nm thick adhesion Ti film and 200 nm thick Au film by ion beam sputtering deposition. Circular grooves of either 5 or 10 μm in diameter and 90 - 100 nm in width were milled into the gold film by gallium focused ion beam (FIB, Tescan Lyra3). For excitation of SPPs at the grooves, we used linearly polarized light originating from a He-Ne laser (633 nm, output power 50 mW). The phase of the light was controlled by a spatial light modulator (LCOS-SLM, Hamamatsu X10468-01). The SLM enables us to alter the phase of the light (in the range from 0 to 2π) in well-defined parts of the beam upon the its reflection from an optically active liquid crystal chip of SLM. Light reflected from SLM entered a Nanonics Multiview 4000 (see Fig. 1f) scanning near field optical microscope (SNOM) system and was focused on the slits from the bottom side of the sample by 50 \times objective (Nikon, NA 0.45, long working distance). This system is equipped with 3D piezoelectric sample holder which enables to precisely align the groove with the fo-

cused beam of incident light in order to achieve homogeneous illumination of the groove. The SPPs interference pattern was acquired by Au coated commercial SNOM SiO₂ fiber tips with the 50 nm aperture size connected to a photo-multiplier tube (PMT) by a multimodal optical fiber.

4.2 Simulations

Numerical calculations were carried out using a commercial software based on the finite-difference time-domain numerical method (Lumerical FDTD Solutions). For the computations, the optical properties of used materials were taken from internal database, which is based on well-known handbooks of optical constants (for SiO₂ Ref.⁴⁴, for Au Ref.⁴⁵). The borders of simulated area were defined by perfectly matched layers (PML), suppressing reflections of electromagnetic waves back into simulation region. The size of computation mesh cells was set to 10 nm in all three dimensions.

In the simulations, the groove was illuminated from the side of the glass substrate by a white light plane waves in the wavelength range from 500 nm to 800 nm. To simulate the effect of SLM, several identical light sources were used, each of them illuminating a different part of the groove and the required phase shift was set between the sources.

Electromagnetic field was recorded by a planar monitor at the close vicinity of the gold film surface.

Conflicts of interest

There are no conflicts to declare.

Acknowledgements

This work has been supported by the Grant Agency of the Czech Republic (GA15-21581S and GA18-01396S). The research was partially carried out under the project CEITEC 2020 (LQ1601) with a financial support from the Ministry of Education, Youth and Sports of the Czech Republic under the National Sustainability Programme II. Part of the work was carried out with the support of CEITEC Nano Research Infrastructure (ID LM2015041, MEYS CR, 2016–2019), CEITEC Brno University of Technology.

References

- 1 Q. Xu, X. Zhang, Y. Xu, C. Ouyang, Z. Tian, J. Gu, J. Li, S. Zhang, J. Han and W. Zhang, *Laser & Photonics Reviews*, 2017, **11**, 1600212.
- 2 L. Huang, X. Chen, H. Mühlenbernd, H. Zhang, S. Chen, B. Bai, Q. Tan, G. Jin, K.-W. Cheah, C.-W. Qiu, J. Li, T. Zentgraf and S. Zhang, *Nature communications*, 2013, **4**, 2808.
- 3 M. Ozaki, J.-i. Kato and S. Kawata, *Science*, 2011, **332**, 218–220.
- 4 Z. W. Liu, Q. H. Wei and X. Zhang, *Nano Letters*, 2005, **5**, 957–961.
- 5 P. Dvořák, T. Neuman, L. Břínek, T. Šamořil, R. Kalousek, P. Dub, P. Varga and T. Šikola, *Nano Letters*, 2013, **13**, 2558–2563.
- 6 S. I. Bozhevolnyi, V. S. Volkov, E. Devaux, J.-Y. Laluet and T. W. Ebbesen, *Nature*, 2006, **440**, 508–511.
- 7 E. Verhagen, M. Spasenović, A. Polman and L. K. Kuipers, *Physical Review Letters*, 2009, **102**, 203904.
- 8 S. S. Kou, G. Yuan, Q. Wang, L. Du, E. Balaur, D. Zhang, D. Tang, B. Abbey, X.-C. Yuan and J. Lin, *Light: Science & Applications*, 2016, **5**, e16034–e16034.
- 9 P. R. Huft, J. D. Kolbow, J. T. Thweatt and N. C. Lindquist, *Nano Letters*, 2017, **17**, 7920–7925.
- 10 A. Vakil and N. Engheta, *Science*, 2011, **332**, 1291–1294.
- 11 A. Woessner, Y. Gao, I. Torre, M. B. Lundeborg, C. Tan, K. Watanabe, T. Taniguchi, R. Hillenbrand, J. Hone, M. Polini and F. H. L. Koppens, *Nature Photonics*, 2017, **11**, 421–424.
- 12 Y. Xu, Y. Fu and H. Chen, *Nature Reviews Materials*, 2016, **1**, 16067.
- 13 V. M. Shalae, *Nature Photonics*, 2007, **1**, 41–48.
- 14 P. Kolman and R. Chmelík, *Optics Express*, 2010, **18**, 21990–22003.
- 15 J. Babocký, A. Křížová, L. Štrbková, L. Kejik, F. Ligmajer, M. Hrtoň, P. Dvořák, M. Týč, J. Čolláková, V. Křápek, R. Kalousek, R. Chmelík and T. Šikola, *ACS Photonics*, 2017, **4**, 1389–1397.
- 16 P. L. Phillips, J. C. Knight, J. M. Pottage, G. Kakarantzas and P. S. J. Russell, *Applied Physics Letters*, 2000, **76**, 541–543.
- 17 A. Nesci, R. Dändliker and H. P. Herzig, *Optics Letters*, 2001, **26**, 208.
- 18 P. Tortora, M. Abashin, I. Märki, W. Nakagawa, L. Vaccaro, M. Salt, H. P. Herzig, U. Levy and Y. Fainman, *Optics Letters*, 2005, **30**, 2885.
- 19 M. Ayache, M. P. Nezhad, S. Zamek, M. Abashin and Y. Fainman, *Optics Letters*, 2011, **36**, 1869.
- 20 L. Stern, B. Desiatov, I. Goykhman, G. M. Lerman and U. Levy, *Optics Express*, 2011, **19**, 12014.
- 21 A. Nesci and O. J. F. Martin, *Proceedings of SPIE*, 2005, **5928**, 59280U.
- 22 T. Zentgraf, J. Dorfmueller, C. Rockstuhl, C. Etrich, R. Vogelgesang, K. Kern, T. Pertsch, F. Lederer and H. Giessen, *Optics Letters*, 2008, **33**, 848.
- 23 M. Schnell, A. García-Etxarri, A. J. Huber, K. Crozier, J. Aizpurua and R. Hillenbrand, *Nature Photonics*, 2009, **3**, 287–291.
- 24 M. Schnell, P. S. Carney and R. Hillenbrand, *Nature Communications*, 2014, **5**, 3499.
- 25 M. L. M. Balistreri, J. P. Korterik, L. Kuipers and N. F. van Hulst, *Physical Review Letters*, 2000, **85**, 294–297.
- 26 J. Jose, F. B. Segerink, J. P. Korterik, J. L. Herek and H. L. Offerhaus, *Applied Physics A*, 2011, **103**, 673–676.
- 27 N. Rotenberg and L. Kuipers, *Nature Photonics*, 2014, **8**, 919–926.
- 28 J. W. Nelson, G. R. Knefelkamp, A. G. Brolo and N. C. Lindquist, *Light: Science & Applications*, 2018, **7**, 52.
- 29 I. Yamaguchi and T. Zhang, *Optics Letters*, 1997, **22**, 1268.
- 30 D. Malacara, *Optical Shop Testing*, Wiley, 2007, p. 888.
- 31 A. Kubo, N. Pontius and H. Petek, *Nano Letters*, 2007, **7**, 470–475.
- 32 G. Spektor, D. Kilbane, A. K. Mahro, B. Frank, S. Ristok, L. Gal,

- P. Kahl, D. Podbiel, S. Mathias, H. Giessen, F.-J. Meyer zu Heringdorf, M. Orenstein and M. Aeschlimann, *Science*, 2017, **355**, 1187–1191.
- 33 P. Lalanne, J. P. Hugonin and J. C. Rodier, *Physical Review Letters*, 2005, **95**, 263902.
- 34 H. Kim and B. Lee, *Optics Express*, 2008, **16**, 8969.
- 35 Z. Liu, J. M. Steele, W. Srituravanich, Y. Pikus, C. Sun and X. Zhang, *Nano Letters*, 2005, **5**, 1726–1729.
- 36 B. le Feber, N. Rotenberg, D. M. Beggs and L. Kuipers, *Nature Photonics*, 2013, **8**, 43–46.
- 37 N. Rotenberg, M. Spasenović, T. L. Krijger, B. le Feber, F. J. García de Abajo and L. Kuipers, *Physical Review Letters*, 2012, **108**, 127402.
- 38 P. Dvořák, Z. ědes, M. Kvapil, T. Šamořil, F. Ligmajer, M. Hrtotň, R. Kalousek, V. Křápek, P. Dub, J. Spousta, P. Varga and T. Šikola, *Optics Express*, 2017, **25**, 16560.
- 39 M. Born and E. Wolf, *Principles of Optics*, Cambridge University Press, 1999, p. 985.
- 40 B. Gjonaj, J. Aulbach, P. M. Johnson, A. P. Mosk, L. Kuipers and A. Lagendijk, *Nature Photonics*, 2011, **5**, 360–363.
- 41 Z.-B. Zheng, J.-T. Li, T. Ma, H.-L. Fang, W.-C. Ren, J. Chen, J.-C. She, Y. Zhang, F. Liu, H.-J. Chen, S.-Z. Deng and N.-S. Xu, *Light: Science & Applications*, 2017, **6**, e17057.
- 42 D. Wintz, K. Chaudhary, K. Wang, L. A. Jauregui, A. Ambrosio, M. Tamagnone, A. Y. Zhu, R. C. Devlin, J. D. Crossno, K. Pistunova, K. Watanabe, T. Taniguchi, P. Kim and F. Capasso, *ACS Photonics*, 2018, **5**, 1196–1201.
- 43 J. Lin, J. Dellinger, P. Genevet, B. Cluzel, F. de Fornel and F. Capasso, *Physical Review Letters*, 2012, **109**, 093904.
- 44 E. D. Palik, *Handbook of Optical Constants of Solids*, Academic Press, 1st edn, 1991, p. 1096.
- 45 P. B. Johnson and R. W. Christy, *Physical Review B*, 1972, **6**, 4370–4379.